



Influence of Channel-Spanning Engineered Logjam Structures on Channel Hydrodynamics

S. Müller¹ , E. M. Follett¹ , P. Ouro², and C. A. M. E. Wilson¹ 

¹Hydro-Environmental Research Center, School of Engineering, Cardiff University, Cardiff, UK, ²School of Mechanical, Aerospace and Civil Engineering, University of Manchester, Manchester, UK

Key Points:

- We experimentally investigated the impact of six non-porous and porous engineered logjams on upstream and downstream channel hydrodynamics
- Main gap below logjams produced a wall jet, with maximum jet velocity dependent on channel blockage
- Highly turbulent near wake observed for non-porous and short logjams, with long porous jams characterized by lower turbulent kinetic energy

Supporting Information:

Supporting Information may be found in the online version of this article.

Correspondence to:

S. Müller,
MullerS1@Cardiff.ac.uk

Citation:

Müller, S., Follett, E. M., Ouro, P., & Wilson, C. A. M. E. (2022). Influence of channel-spanning engineered logjam structures on channel hydrodynamics. *Water Resources Research*, 58, e2022WR032111. <https://doi.org/10.1029/2022WR032111>

Received 4 FEB 2022
Accepted 22 NOV 2022

Author Contributions:

Conceptualization: S. Müller, E. M. Follett, C. A. M. E. Wilson
Data curation: S. Müller, E. M. Follett
Formal analysis: S. Müller, E. M. Follett, P. Ouro
Funding acquisition: E. M. Follett, C. A. M. E. Wilson
Investigation: S. Müller
Methodology: S. Müller, E. M. Follett, C. A. M. E. Wilson
Supervision: E. M. Follett, P. Ouro, C. A. M. E. Wilson
Visualization: S. Müller, E. M. Follett, P. Ouro
Writing – original draft: S. Müller, E. M. Follett

© 2022. The Authors.

This is an open access article under the terms of the [Creative Commons Attribution License](https://creativecommons.org/licenses/by/4.0/), which permits use, distribution and reproduction in any medium, provided the original work is properly cited.

Abstract Nature-based solutions to flood risk management, such as engineered logjams (ELJs), contribute to the reintroduction of wood in rivers. As part of stream restoration, and utilized in tributaries, ELJs increase upstream water levels, causing the flow to spill onto surrounding floodplains, resulting in the desynchronization of peak flows in a river network. To understand the effect of ELJs on local river hydrodynamics, we experimentally investigate the flow field upstream and downstream of six ELJs, using acoustic Doppler velocimetry and flow visualization. We consider channel-spanning structures designed with a gap (b_0) underneath, allowing unhindered baseflow. Our results revealed that upstream of the logjams, flow diverted toward the lower gap, creating a primary jet exiting underneath the structures, whose strength depends on the physical logjam design. Maximum jet velocities remained constant until a downstream distance of $4b_0$ for all logjams. The upper wake was structure-dependent, with logjam structures allowing distinct internal flow paths generating secondary jets, which influenced near wake decay ($x < 4b_0$) and turbulent mixing. The highest turbulence in the near wake was found for the non-porous and short, porous logjam designs, while the upper wake of all long, porous logjams was characterized by low turbulent kinetic energy levels. Far wake decay ($x > 4b_0$) was self-similar for all logjams and resulted in near flow recovery at downstream streamwise distances greater than $35b_0$. ELJs are likely to enhance bed shear stress, increasing the risk of local scour and sediment mobilization. Our study expands the current knowledge of ELJ hydrodynamics and highlights potential implications for the riverine ecosystem.

Plain Language Summary Engineered logjams (ELJs) with a lower gap are a nature-based solution for flood risk management and river restoration. Channel-spanning wooden logjams increase upstream water levels, causing the flow to spill onto surrounding floodplains, slowing down surface and ground water through the catchment. Using experimental flow velocity measurements in a laboratory open channel flume, we investigated the local flow field upstream and downstream of six ELJs. We demonstrate that the flow blockage caused by ELJs resulted in an increase in upstream flow depth, with a lower velocity at logjam height, and higher velocity at gap height which extended into the downstream region. While this high-velocity stream was present for all logjams with a lower gap, the downstream flow field at logjam height was dependent on logjam design. Porous ELJs allowing flow through the structure, for instance, generated smaller, weaker streams which influenced the flow field. Independent of the logjam design, the flow field recovered to its original, undisturbed flow field at nearly the same downstream distance. Our study highlights the flow alterations associated with different physical logjam designs and raises potential secondary impacts on the riverine ecosystem such as local scouring, sediment mobilization, and trapping as well as the enhancement in habitat complexity.

1. Introduction

The management and understanding of wood in rivers have undergone major transformations over the last four centuries (Wohl, 2014, 2017a). While initially wood was removed to enhance conveyance, navigation, and log transport, the resulting detrimental effects on ecosystem biodiversity initiated its reintroduction, as part of river management programs (Reich et al., 2003; Wohl, 2017a, 2017b). Individual logs, groups of logs (e.g., Zhang et al., 2020a, 2020b), and partial channel-spanning engineered logjams (ELJs) (e.g., Bennett et al., 2015; Gallisdorfer et al., 2014) are now being placed, with the main purpose of restoring aquatic habitats and fish communities (Bisson et al., 2003; Reich et al., 2003) and deflecting flow to reduce bank erosion (Gallisdorfer et al., 2014; Zhang et al., 2020b). The change in perception of wood in rivers has initiated discussion on the hydraulic, hydrological, geomorphological, and ecological effects of wood (e.g., Abbe & Montgomery, 1996; Gregory et al., 2003; Wohl, 2017a).

Writing – review & editing: S. Müller,
E. M. Follett, P. Ouro, C. A. M. E. Wilson

Besides the use of wood for river restoration schemes, the use of channel-spanning ELJs in rivers and streams as nature-based solutions to flood risk management has received much attention during the last 10 yrs (Burgess-Gamble et al., 2018; Dodd et al., 2016; SEPA, 2016) as a result of the increasing number of major floods (Santato et al., 2013) and the expected increase in high intensity rainfall events due to climate change (Jia et al., 2019; Lehman et al., 2015). These porous ELJs, also referred to as leaky barriers, consist of logs, fallen trees, or branches, sourced from the surrounding area. Installed perpendicular to the flow in the mid to upper catchment region (i.e., where channel width is smaller than key log length) (Linstead & Gurnell, 1999), they span the complete width of the river channel, allowing unhindered base flow through a vertical gap between the bottom of the structure and the riverbed (b_0 , Figure 2), as depicted in Müller et al. (2021a) (Figure 1) for an idealized porous (a) and non-porous (b) logjam. Despite this vertical gap, current design guidelines only consider the requirements necessary to facilitate fish movement (Dodd et al., 2016) and disregard the impact of physical logjam design on channel hydrodynamics and alterations to the riverine habitat. Due to their relatively low cost and high ecological benefits, ELJs have gained popularity worldwide (Reich et al., 2003; Strosser et al., 2015; Young, 1991), with a concerted effort made in the UK in monitoring the effectiveness of such measures in reducing flood flows (Burgess-Gamble et al., 2018; Dodd et al., 2016; Forest Research, 2007; Woodland Trust, 2016). A wide range of in-stream, floodplain, and overland structures can be found in sites such as Pickering (North East England), Holnicote (South West England), Shropshire (West England), and Stroud (South West England) (e.g., Burgess-Gamble et al., 2018; National Trust, 2015; Nisbet et al., 2015). In these natural flood management schemes, logjams installed in groups of 100 plus units are used on selected tributaries in the river network sometimes with the key aim of desynchronizing the tributary peak flows from the main river.

Under high flow conditions, when water inundates the logjam vertical extent (Figure 2; $z \geq b_0$), ELJs increase upstream backwater rise, with the aim to increase the connection between the river channel and floodplain. When the upstream water depth rises above the channel bankfull depth, water spills onto the upstream floodplain, using this area for water storage and enhancing infiltration into the ground, which, in turn, leads to the attenuation of the flow reaching the downstream main river (Estrela et al., 2001; Muhawenimana et al., 2020; SEPA, 2016). As the lower channel remains unobstructed (Figure 2, $z \leq b_0$, gap beneath logjams), a portion of the flow passes beneath the structure, while the remaining flow overtops or passes through the logjam. An idealized non-porous logjam mimics the natural accumulation of sediment, leaf material, and wood, causing the flow to diverge around the logjam (Müller et al., 2021a). Flow around a non-porous logjam is analogous to flow passing a bluff body, such as a sluice, weir, and tidal gate, creating a zone of elevated pressure upstream of the logjam which causes the flow to diverge around the structure, leading to an increase in streamwise mean velocity beneath it. While a recirculation region forms immediately downstream of the structure, the high velocity region exiting the logjam act like a modified wall jet (Figure 1b in Müller et al., 2021a; Ead & Rajaratnam, 2002). This jet maintains its maximum velocity until a downstream distance of $x/b_0 = (4U_0/U_{\text{jet,max}})^2$ before commencing a rapid decay (Bhuiyan et al., 2011; Ead & Rajaratnam, 2002).

In the case of the porous structure (Figure 1a in Müller et al., 2021a), the jet exiting the logjam is anticipated to decrease in strength due to the increased proportion of flow passing through the logjam. Depending on the logjam's physical structure and log arrangement, flow passing through the logjam creates smaller and weaker offset jets (Müller et al., 2021a), and a multiple jet configuration. The interaction between a wall jet and an offset jet, or between two or more parallel jets, is characterized by three distinct regions (Figure 2; Daubner et al., 2018; Fujisawa et al., 2004; Wang & Tan, 2007). Within the converging region, the parallel jets start to deflect toward each other and create a recirculation zone in between the jets. In the merging region, both jets gradually merge with increasing downstream distance until finally reaching the combined region in which both jets behave like a single one (Wang & Tan, 2007). While the near wake of multiple jets is characterized by the shedding of Kármán-like vortices in the inner shear layer, the free shear layer of a single jet, either offset or wall jet, is characterized by Kelvin–Helmholtz roll-ups (Wang & Tan, 2010).

In addition, the potential generation of multiple jets by some ELJ designs, and the flow around some ELJ structures also exhibit similarities to the flow around horizontal cylinder configurations, which have been of specific interest due to their wide engineering application. While single horizontal cylinders have been studied experimentally (Kahraman et al., 2012; Muhawenimana et al., 2020) and numerically (Lehmkuhl et al., 2013; Nishino et al., 2008; Ouro et al., 2019), only a few studies examine the flow field around multiple horizontal cylinders, with those studies focusing on four in-line square (e.g., Lam & Lo, 1992; Wang & Tan, 2012; Zou et al., 2008), and staggered configurations (Lam et al., 2003; Lam & Zou, 2009; Zou et al., 2011). Despite the useful insights

of these studies, the majority of these studies have only been conducted for low Reynolds numbers ($Re_d < 2,100$), which limits the applicability of these studies to the understanding of the hydrodynamics of full-scale ELJs in fully turbulent flows, with the exception of the study by Lam and Zou (2009), which was conducted for $11,000 < Re_d < 20,000$.

In this study, the upstream flow diversion and downstream wake hydrodynamics of six idealized ELJs intended to be used as flood risk mitigation measures were investigated through acoustic Doppler velocimetry measurements and dye visualization. A conceptual logjam model was employed to examine the impact of structure void ratio on the interaction of the wall jet from the flow underneath the logjam, and the weaker offset jets generated from the logjam structure. The vertical gap between the bed and the logjam was maintained, while the log configuration and log number varied to generate different flow paths and offset jet characteristics. First and second-order turbulence statistics as well as jet development and decay were analyzed. Furthermore, scaling effects were investigated for one logjam design using two flumes at different scales. Through the use of experimental evidence, this study aims to provide guidance on how the physical design of ELJs may alter channel hydrodynamics and what consequences these alterations have on channel geomorphology and fish movement.

2. Methods

Upstream and downstream hydrodynamics were measured for six ELJ in two flumes, including five physical designs and one scaled logjam. In the following, flume setup, logjam characteristics, and hydrodynamic measurement methods are explained.

2.1. Flume Setup

Experiments were conducted for five logjam configurations (S1–S5) in a recirculating open channel flume (hereafter denoted as Flume 1) which was 10 m long (L_{flume}), 1.2 m wide (B_{flume}), and 0.3 m deep (H_{flume}), with the longitudinal bed slope was set to 0.001 m/m (Figure 1a). The flume had a symmetrical compound channel section, with a rectangular main channel of width 0.6 m (B_{mc}) and total floodplain width of 0.6 m ($2B_{\text{fp}}$). The main channel had a bankfull depth of 0.15 m (H_{mc}). A detailed visualization of the described flume characteristics can be found in Figure 2 given in the study by Müller et al. (2021a). Prior to the installation of a logjam, uniform subcritical flow conditions were established for the bankfull flow condition, relating to a discharge (Q) of $0.028 \text{ m}^3\text{s}^{-1}$ and a flow depth (h) of 0.15 m (open channel velocity profile at $x/b_0 = 0.8$ shown in Müller et al., 2021b). The discharge and tailgate weir height remained fixed for the subsequent logjam experiments. The installation of the logjam resulted in a change in the water surface profile upstream of the logjam, generating gradually varied flow conditions and a backwater rise (Figure 2), causing the flow to spill onto the adjacent flood plain in Flume 1. Flow depth was measured using a Vernier pointer gauge with an accuracy of $\pm 0.1 \text{ mm}$ and an ultrasonic flowmeter (TecFluid Nixon CU100) measured the discharge to a precision of $\pm 1.5\%$.

To examine scale effects and the impact of Reynolds number, a generalized 1:2 scale test was carried out for one logjam configuration (scaled logjam S6) in a larger flume (hereafter denoted as Flume 2; Figure 1b). Flume 2 was 17 m long, 1.2 m wide, and 1.0 m deep and equipped with a rectangular cross-section. Due to the absence of lateral floodplains, there was no overbank flow. The Froude scaling law was used, and the bulk velocity was scaled to maintain a Froude number ($Fr = U_0/\sqrt{gh}$) equal to 0.25 between comparative tests, corresponding to a discharge of $Q = 0.157 \text{ m}^3\text{s}^{-1}$ and flow depth of $h = 0.3 \text{ m}$.

For both flumes, the flow direction was defined as the positive x direction, with y and z the lateral and vertical coordinates, respectively, as indicated in Figure 1. For the data analysis, the upstream and downstream edges of the logjam were defined as $x = 0$ for $x < 0$ and $x > 0$, respectively, as indicated in Figure 2.

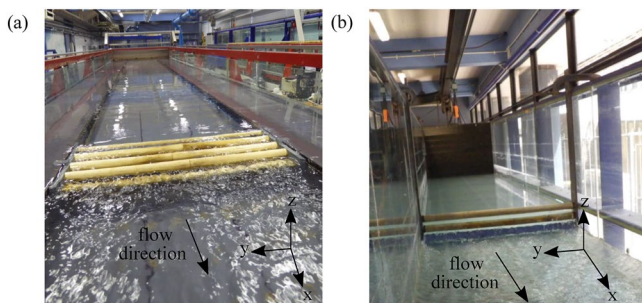


Figure 1. (a) Open channel Flume 1, showing the experimental setup for the five logjam designs S1-5 and (b) Flume 2, showing logjam S6, which was a generalized 1:2 scale test of S5; photographs looking in upstream direction.

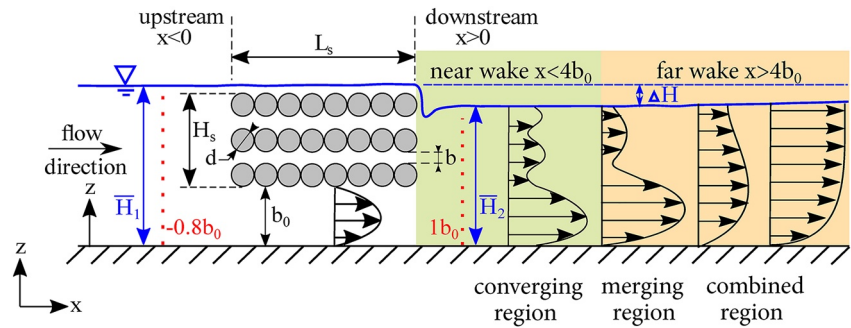


Figure 2. Schematic diagram depicting an idealized logjam of height H_s and longitudinal length L_s with vertical inter-cylinder gaps (b) and a vertical gap between the structure and the channel bed (b_0). The structure is composed of horizontal logs of diameter (d) aligned parallel to the channel bed and normal to the flow direction. Upstream and downstream edge of the logjam defined as $x = 0$ for $x < 0$ and $x > 0$, respectively. Immediate upstream ($x/b_0 = -0.8$, $x/H_s = -0.4$ for S1–5) and downstream ($x/b_0 = 1$, $x/H_s = 0.5$ for S1–5) ADV measurement locations are indicated in red. Near-wake ($x < 4b_0$, $x < 2H_s$) and far wake ($x > 4b_0$, $x > 2H_s$) are indicated in green and orange areas, respectively. Water surface profile is indicated in blue, with \bar{H}_1 and \bar{H}_2 depicting mean upstream and downstream flow depth, and ΔH being the backwater rise (Figure amended from Müller et al., 2021a).

2.2. Engineered Logjam Models

The main characteristics of all six ELJ are depicted in Figure 2, comprising the number of logs (n) with a diameter (d), longitudinal extension (L_s), logjam height (H_s), inter-log gaps (b) and vertical gap between the structure and the channel bed (b_0).

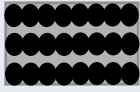
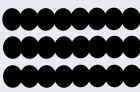
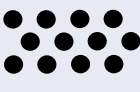
Logjam structures S1–S5 were constructed from wooden logs of diameter (d) 25 mm with a structure height (H_s) of 100 mm, while the scaled ELJ S6 was constructed using logs of diameter (d) 50 mm and occupied a vertical height (H_s) of 200 mm. Each log was aligned perpendicular to the main flow direction spanning the complete width of the main channel (Figure 1), that is, $B_{mc} = 0.6$ m for case S1 to S5 and $B_{mc} = 1.2$ m for case S6. A vertical gap of $b_0 = 50$ and 100 mm (for S1–S5 and S6, respectively) was created between the flume bed and the lowest log, remaining fixed for all configurations. The six logjams include a non-porous structure S1, analogous to a bluff body, of length $L_s = 8d$ for which the structure was wrapped in polyethylene to ensure its impermeability; a porous structure S2 with three log rows, length $L_s = 8d$ and void ratio ($\Phi = 41.1\%$); S3 is a staggered configuration with a greater inter-log gap and higher void ratio ($\Phi = 70.5\%$); S4 is another staggered logjam with a closer inter-log gap and lower void ratio than S3 ($\Phi = 55\%$); and S5 and S6 are short length structures ($L_s = 1d$) composed of three horizontal logs vertically aligned.

It should be noted that the investigated ELJs (S1–6) were not scaled to mimic specific prototypes found in the field but rather to represent a subset of possible physical ELJ designs of varying characteristics, and to investigate their impact on local channel hydrodynamics. The geometric scale of the logjams used in this study, however, corresponds to an approximate scale of 1:7 compared to ELJs installed on the Wilde Brook test reach in Corvedale (Shropshire, UK; Follett & Wilson, 2020). Further details of how the chosen discharge and geometric scale agree with logjams found in the field can be found in Müller et al. (2021b).

A summary of the experimental details of all logjams is given in Table 1, including frontal projected area (A_p ; $A_p = B_{mc}H_s$ for S1 and S4, and $A_p = nB_{mc}d$ for S2–3 and S5–6), logjam void ratio ($\Phi = V_{\text{void}}/V_{\text{control}}$) calculated from the ratio of the pore volume ($V_{\text{void}} = V_{\text{control}} - V_{\text{solid}}$), with V_{solid} being the volume occupied by the solid logjam ($\pi(d/2)^2nB_{mc}$) and $V_{\text{control}} = B_{mc}H_sL_s$ (no logjam present), and relative channel void area $A_{rv} = 1 - A_p/(B_{mc}H_{mc})$, calculated from the bankfull channel area $B_{mc}H_{mc}$ relative to logjam projected area A_p . Table 1 also provides experimental details for each test, including flow discharge (Q), upstream flow depth (\bar{H}_1) measured immediately upstream of all logjams ($x/b_0 = -0.6$) and the difference between mean upstream (\bar{H}_1) and downstream (\bar{H}_2) flow depths (ΔH), with \bar{H}_1 and \bar{H}_2 being calculated from the average of all water elevation measurements upstream and downstream, respectively. Upstream bulk velocity was computed as $U_0 = Q/(\bar{H}_1 B_{mc})$ or in the case of overbank flow as $U_0 = Q/(H_{mc}B_{mc} + B_{\text{flume}}(\bar{H}_1 - H_{mc}))$. Reynolds number was calculated based on the log diameter ($Re_d = U_0d/\nu$).

Table 1

Experimental Details for the Five Logjam Tests (S1-5) Conducted in Flume 1 and the Scaling Test (S6) Conducted in Flume 2, Including Number of Logs (n), Longitudinal Logjam Length (L_s), Logjam Height (H_s), Vertical Gap (b_0), Frontal Projected Area (A_p), Logjam Void Ratio (Φ), Relative Channel Void Area A_{rv} , Discharge (Q), Upstream Flow Depth H_1 , Backwater Rise (ΔH), Upstream Bulk Velocity (U_0) and Reynolds Number (Re_d)

Logjam structure	n [-]	L_s [mm]	H_s [mm]	b_0 [mm]	A_p [m ²]	Φ [%]	A_{rv} [-]	Q [m ³ s ⁻¹]	H_1 [mm]	ΔH [mm]	U_0 [m/s]	Re_d [-]
S1 	24	200	100	50	0.06	0	0.33	0.028	173.0	32.7	0.24	6,000
S2 	24	200	100	50	0.05	41.1	0.43	0.028	160.0	16.0	0.28	7,000
S3 	12	200	100	50	0.05	70.5	0.43	0.028	161.5	15.7	0.27	6,750
S4 	15	175	100	50	0.06	55.0	0.33	0.028	161.5	27.6	0.27	6,750
S5 	3	25	100	50	0.05	41.1	0.43	0.028	158.0	9.6	0.29	7,250
S6 	3	50	200	100	0.18	41.1	0.5	0.157	*	*	0.44	22,000

Note. *Flow Depth was not measured for the scaled logjam S6.

2.3. Data Collection

Data on upstream and downstream hydrodynamics for all ELJ were collected using acoustic Doppler velocimetry (ADV) measurements and flow visualization.

2.3.1. ADV Measurements

The upstream flow diversion and downstream wake hydrodynamics were examined by measuring the three components of velocity using a sideways-looking ADV (Nortek Vectrino, Nortek AS 2009). Spherice[®] 110P8 hollow glass spheres with a mean particle size of 11.7 μm and a specific gravity of 1.10 g/cc (Potters Industries LLC) were added to the water to enhance the ADV signal. Measurements were carried out at a sampling rate of 200 Hz for 300–1,800 s depending on the data quality. The sufficiency of the sampling period length was checked by analyzing the cumulative time average of the measurements and the root mean square velocity fluctuations ($\sqrt{u'^2}$) over the sampling period. We found that in the near wake region immediately downstream of the logjam, the sampling duration needed to be increased significantly up to 12,00 and 1,800 s for S1–S5 and S6, respectively, to capture a representative sample of the high-frequency turbulent fluctuations and obtain data of sufficient quality. Measurement data were filtered and post-processed using Matlab (2018). In the first pre-filtering step, velocity data with thresholds below 15 dB and 70% for Flume 1 and 10 dB and 70% for Flume 2 for SNR and Correlation, respectively, were removed (Nortek AS, 2009; Nortek Support Center, 2019). In a second step, an open-source toolbox was implemented to despiking the data (Mori, 2020; Mori et al., 2007), using a despiking algorithm based on the three-dimensional phase space method introduced by Goring and Nikora (2002) and modified by Wahl (2002). The velocity records were decomposed into time-averaged and fluctuating components ($u = \bar{u} + u'$), respectively,

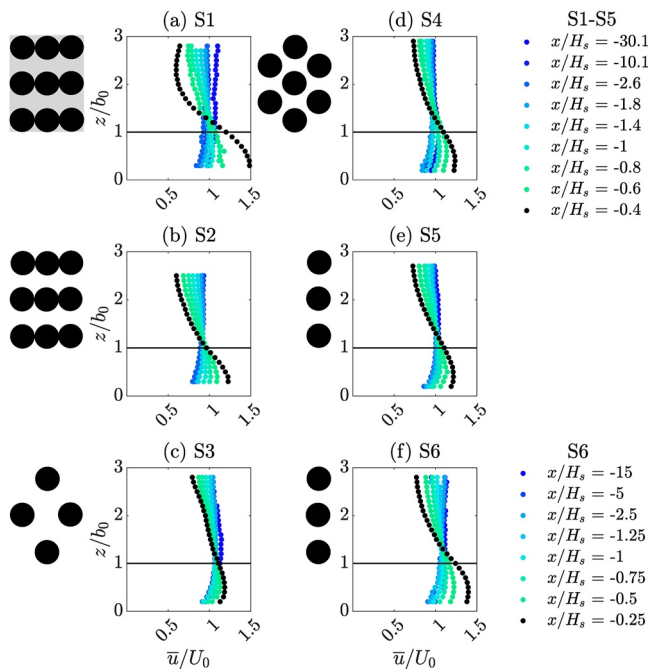


Figure 3. Progression of upstream mean streamwise velocity profiles (\bar{u}) normalized by the bulk velocity (U_0), depicting selected profiles measured between the furthest upstream profile (S1–5: $x/H_s = -30.1$; S6: $x/H_s = -15$) and the profile measured close to the logjam’s upstream edge (S1–5: $x/H_s = -0.4$; S6: $x/H_s = -0.25$). Longitudinal velocity profile location (x) was normalized by the logjam height (H_s) of 100 mm for S1–5 and 200 mm for S6. Only half of the logjam structures S1 to S4 is shown on the left-hand side of the contour plot to indicate their vertical location. An increase in streamwise velocity was observed below the structure’s bottom edge ($z/b_0 = 1$, black horizontal line) due to flow diversion underneath structures. Vertical extent of recorded velocity profiles may vary due to longitudinal changes in upstream flow depth.

denoted by an overbar and prime operation. Turbulent kinetic energy was calculated as $\text{tke} = \frac{1}{2} (\overline{u'^2} + \overline{v'^2} + \overline{w'^2})$.

For S1–S5, 26 velocity profiles, including 14 profiles upstream and 12 profiles downstream, were measured along the channel centerline, starting at $-0.8b_0$ and $1b_0$ upstream and downstream of the logjam, respectively (Figure 2). For approx. $4b_0$ upstream and downstream of the logjam, velocity profiles were equally spaced by 20 mm ($0.4b_0$) in the longitudinal direction. As the distance away from the logjam increased, this longitudinal resolution increased to 60 mm ($1.2b_0$), 100 mm ($2b_0$), 250 mm ($5b_0$), 500 mm ($10b_0$), and 1,000 mm ($20b_0$) between velocity profiles (see Figure S1). In the vertical direction, up to 26 points were measured, equally spaced by 5 mm and starting at between 10 and 15 mm from the flume bed until approximately 30 mm below the water surface, due to physical constraints of the ADV (i.e., submergence of the acoustic transmitter at all times). For the larger scale model (S6), eight upstream profiles and 15 downstream profiles were measured starting at 20 mm above the flume bed until approximately 30 mm below the water surface with a vertical spatial resolution of 10 mm. Measurements started $30b_0$ upstream and finished $50b_0$ downstream of S6, with velocity profiles equispaced by 50 mm ($0.5b_0$) between 0.5 and $2.5b_0$ upstream and downstream of the logjam. With increasing distance away from the logjam, longitudinal spacing between velocity profiles increased to 100 mm ($1b_0$), 150 mm ($1.5b_0$), 250 mm ($2.5b_0$), 500 mm ($5b_0$), 1,000 mm ($10b_0$), and 2,000 mm ($20b_0$). A figure depicting the ADV measurement locations in Flume 1 and 2 can be found in the Cardiff University data catalog (<http://doi.org/10.17035/d.2021.0131419068>) and the Figure S1.

2.3.2. Flow Visualization

The flow patterns and turbulence structure of the near wake field were visualized for each logjam configuration. Fluorescent Fwt red and Flt yellow with green dye (Cole-Parmer Instrument Company Ltd) were injected along the centerline at the upstream edge of the logjam at multiple elevations. A GoPro Hero 5 underwater camera was positioned on the left-hand side of the main channel wall of Flume 1 and a Nikon D3300 camera was mounted on the glass flume sidewall of Flume 2.

3. Results

3.1. Upstream Hydrodynamics

Logjam presence caused a change in the water surface profile and an increase in upstream water depth, or backwater rise (ΔH). The increase in backwater rise was highest for S1 and S4, the logjams with the highest frontal projected area (A_p , Table 1). Upstream water depth increased with proximity to the logjams and caused the flow to spill onto the floodplains (Figure 2a), with deeper floodplain inundation observed for logjams with higher cross-sectional blockage. At $x/H_s = -0.3$, the difference between the upstream water surface elevation and main channel height ($H_1 - H_{mc}$) for each logjam design was 23.0 mm (S1), 10.0 mm (S2), 11.5 mm (S3), 11.5 mm (S4), and 8 mm (S5). Floodplain inundation for the non-porous design (S1) was approximately 2–2.3 times greater compared to the long, porous logjams (S3–4). Despite the decrease in logjam length in the case of S5, floodplain inundation was only 20% lower compared to its longer counterpart (S2).

To characterize the upstream flow, mean streamwise velocity profiles (\bar{u}) normalized by the bulk velocity U_0 (Table 1) are presented in Figures 3a–3f for all logjam structures (S1–S6), respectively. Vertical flow diversion toward the structure lower gap ($0 \leq z/b_0 \leq 1$) occurred with increasing proximity to all logjams. An increase in mean streamwise velocity was observed over the vertical extent of the logjams’ lower gap ($z/b_0 < 1$). An inflection point in the vertical profile of mean longitudinal velocity $\bar{u}(z)$ was observed at the height of the lowest log

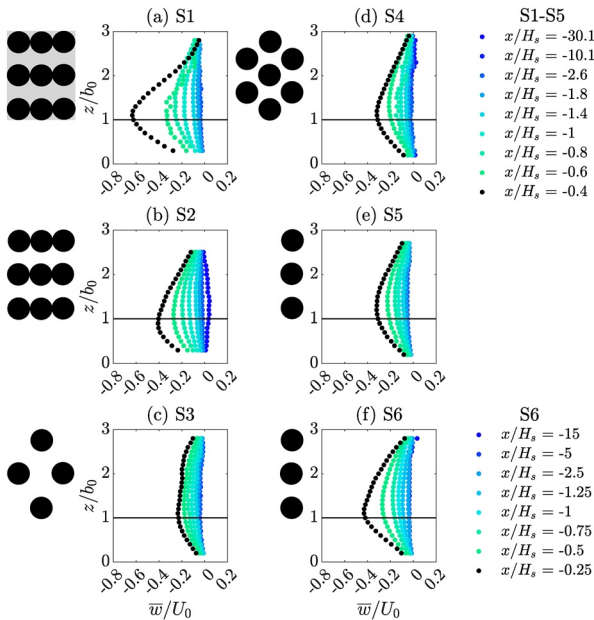


Figure 4. Progression of upstream mean vertical velocity profiles (\bar{w}) normalized by the bulk velocity (U_0), depicting selected profiles measured between the furthest upstream profile (S1-5: $x/H_s = -30.1$; S6: $x/H_s = -15$) and the profile measured close to the logjam's upstream edge (S1-5: $x/H_s = -0.4$; S6: $x/H_s = -0.25$). Longitudinal velocity profile location (x) was normalized by the logjam height (H_s) of 100 mm for S1–5 and 200 mm for S6. Only half of the logjam structures S1 to S4 is shown on the left-hand side of the contour plot to indicate their vertical location. An increase in vertical velocity was observed at height of the lowest logjam edge ($z/b_0 = 1$, black horizontal line) due to flow diversion underneath structures. Vertical extent of recorded velocity profiles may vary due to longitudinal change in upstream flow depth.

($z/b_0 \approx 1-1.5$), followed by a decrease in \bar{w}/U_0 with increasing proximity to the water surface. The change in velocity profile along the channel center was reflected by a change in depth-average mean streamwise velocity ($\langle \bar{u} \rangle$) when comparing the furthest upstream velocity profile with the one measured closest to the upstream logjam (S1-5: $\langle \bar{u}_{x/H_s=-30.1} \rangle / \langle \bar{u}_{x/H_s=-0.4} \rangle$, S6: $\langle \bar{u}_{x/H_s=-15} \rangle / \langle \bar{u}_{x/H_s=-0.25} \rangle$). This comparison showed a 12.7%, 5.2%, 6.5%, 3.3%, 5.6%, and 3.7% decrease $\langle \bar{u} \rangle$ for S1-6. For all logjams, the onset of significant longitudinal flow diversion ($\max(\bar{u}/\bar{u}) > 10\%$) occurred at approx. $-x/H_s > 0.6$ ($x/b_0 \approx -1.2$), with the largest mean longitudinal velocity value obtained for those logjams with the largest blockage and corresponding lowest void ratio, S1 and S4. Furthermore, the profile just upstream of the S1 logjam indicates there is a notable velocity reduction before impinging the structure as this design is non-porous and, unlike the other designs, flow cannot penetrate through it.

Profiles of normalized vertical velocities (\bar{w}/U_0) upstream of the logjams are presented in Figures 4a–4f. A vertical acceleration of the flow occurred when approaching the logjam, with maximum \bar{w}/U_0 observed near the height of the lowest log ($0.9 \leq z/b_0 \leq 1.5$). The largest magnitude \bar{w}/U_0 velocities were obtained for the non-porous logjam S1 ($\bar{w}/U_0 = -0.63$), while values of \bar{w}/U_0 for the porous logjams S2-6 were 35.5%, 95.1%, 97.6%, 89.4%, and 93.7% lower compared to S1, respectively.

3.2. Downstream Hydrodynamics

The instantaneous flow field immediately downstream of all logjams was observed using flow visualization, with rhodamine dye injected at the logjam upper edge midway through the logjam longitudinal extent. The downstream wake of all logjams was characterized by the formation of a fast jet exiting the main gap between the bed ($z = 0$) and structure lower edge ($z/b_0 = 1$), and a structure-dependent upper wake region ($z/b_0 > 1$). Differences in the upper wake characteristics are shown in Figure 5 for the non-porous logjam S1 (a) and two porous logjams S2 (b) and S4 (c). The interface between the primary jet and upper wake regions is shown by the lowest extent of rhodamine dye injected in Figures 5a–5c.

The large cross-sectional blockage of the non-porous logjam (S1) caused water to progress over the upper surface of the structure (Figure 5a). Upon exiting the structure, this overflow stream plunged downwards along the logjam trailing edge until encountering the primary jet, shown by a pronounced line between the lower and upper wake (Figure 5a). In contrast, the provision of inter-log gaps in the case of the porous logjams (S2-6) resulted in reduced backwater rise and water progressing over the upper surface of the logjams (Figures 5b and 5c). The flow

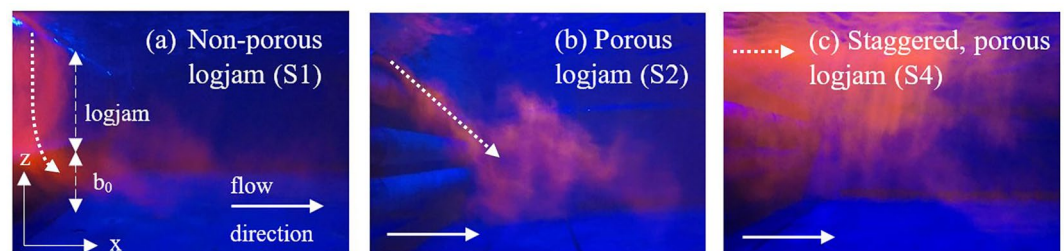


Figure 5. Pathways of water overtopping the logjam (dotted arrow) shown with rhodamine dye injected at the upper edge of non-porous (S1, (a)) and two porous (S2, (b); S4, (c)) logjams. Strong plunging overtopping flow was observed for S1; flow exiting the porous structures show the influence of flow progressing through the structure and log-scale turbulent mixing (S2, similar for S5-S6; and S4, similar for S3). Downstream edge of all logjams is located at the left side of the picture and flow is from left to right.

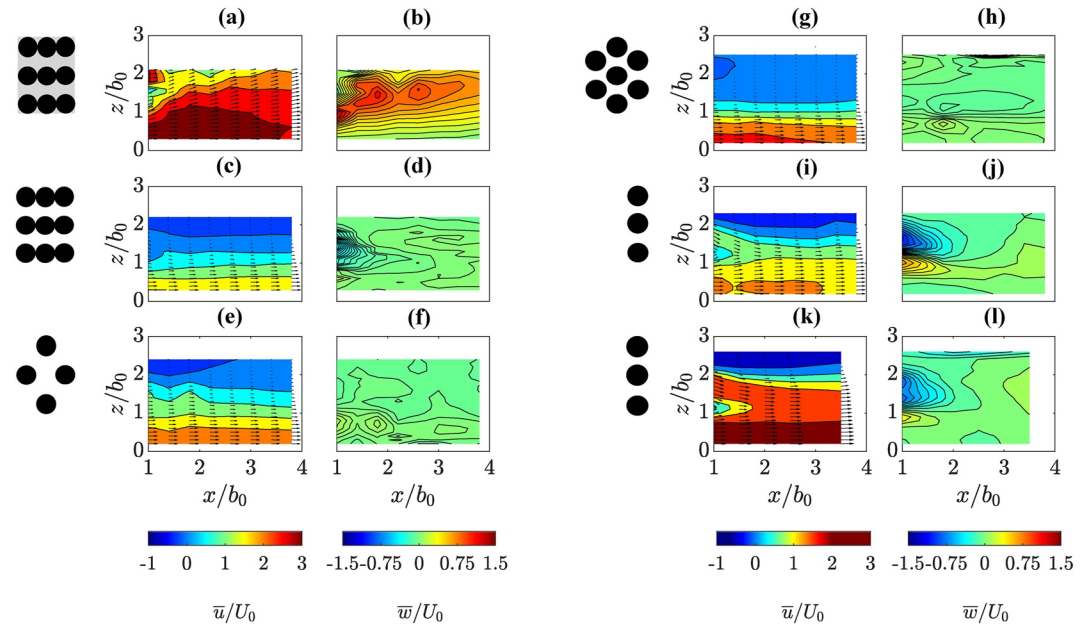


Figure 6. Contours of mean streamwise (\bar{u}/U_0) and vertical (\bar{w}/U_0) velocity normalized by bulk velocity U_0 along the main channel centerline (x - z plane) downstream of all logjams; S1 [a, b], S2 [c, d], S3 [e, f], S4 [g, h], S5 [i, j] and S6 [k, l]. Only half of the logjam structures S1 to S4 is shown on the left hand side of the contour plot to indicate their vertical location.

overtopping logjams with distinct flow through paths (S2, S5-6) was carried in the downstream and downward direction by the flow exiting the structures as shown in the case of S2 (Figure 5b). In contrast, flow overtopping the logjams without distinct flow through paths (S3-4) was predominantly transported in the downstream rather than downward direction due to the absence of secondary jets which created a low-momentum region (Figure 5c).

3.2.1. Near Wake Region

The implications of physical logjam design on the lower ($z/b_0 < 1$) and upper ($z/b_0 > 1$) near wake regions ($x/b_0 < 4$), as observed in Figure 5, are presented in greater detail in Figures 6 and 7, showing contours of normalized mean streamwise (\bar{u}/U_0) and vertical (\bar{w}/U_0) velocities, turbulent kinetic energy (tke/U_0^2), and vertical Reynolds shear stress ($\overline{u'w'}/U_0^2$), respectively.

The lower near wake region of all logjams is characterized by the formation of a primary jet exiting the region underneath the structure ($z/b_0 \leq 1$). The lower near wake region of high momentum flow extends between the flume bed and logjam lower edge. Within this region, longitudinal velocity dominated over the vertical velocity components, with values for $\langle \bar{u} \rangle / U_0$ being 79.9%, 104.4%, 102.9%, 101.1%, 105.2%, and 102.5% for higher compared to $\langle \bar{w} \rangle / U_0$ for S1-6, respectively (i.e., $u \gg w$, $x/b_0 = 1$, Figures 6a, 6c, 6e, 6g, 6i, and 6k). The magnitude of diverted flow varied with the structure's physical characteristics. Immediately downstream of the logjam ($x/b_0 = 1$), the highest \bar{u}/U_0 was found for the non-porous logjam S1, while maximum velocity magnitude were 35.4%, 25.1%, 18.3%, and 34.4% lower for the porous logjams S2-5, respectively [$(z/b_0 (\bar{u}/U_0)_{\max})$]; S1: (0.3, 3.11); S2: (0.2, 2.01); S3: (0.2, 2.33); S4: (0.3, 2.54); S5: (0.4, 2.04); S6: (0.8, 2.30)]. Scaling the short, porous jam (S5) resulted in an 11.3% higher maximum velocity magnitude for S6. Streamwise velocities decreased vertically, with minimum \bar{u}/U_0 found at the highest measurement point, shown by the blue-green contours in Figures 6a, 6c, 6e, 6g, 6i, and 6k.

Immediately downstream of all porous logjams (S2-4) at $x/b_0 = 1$, the value of $d\bar{u}/dz$ at the vertical location of the shear layer between the lower and upper near wake regions ($z/b_0 \approx 1$; Figures 7d, 7f, and 7h) was -0.01 , -0.01 , and -0.02 for S2-4, respectively (Figures 6c, 6e, 6g). The strength of shear at this vertical elevation is reflected in the mixing between the slower flow exiting the logjam upper wake region and flow exiting the lower gap (b_0) for logjams S2-4, shown by the vertical location of peak magnitude of tke/U_0^2 (Figures 7c, 7e, and 7g) and a change

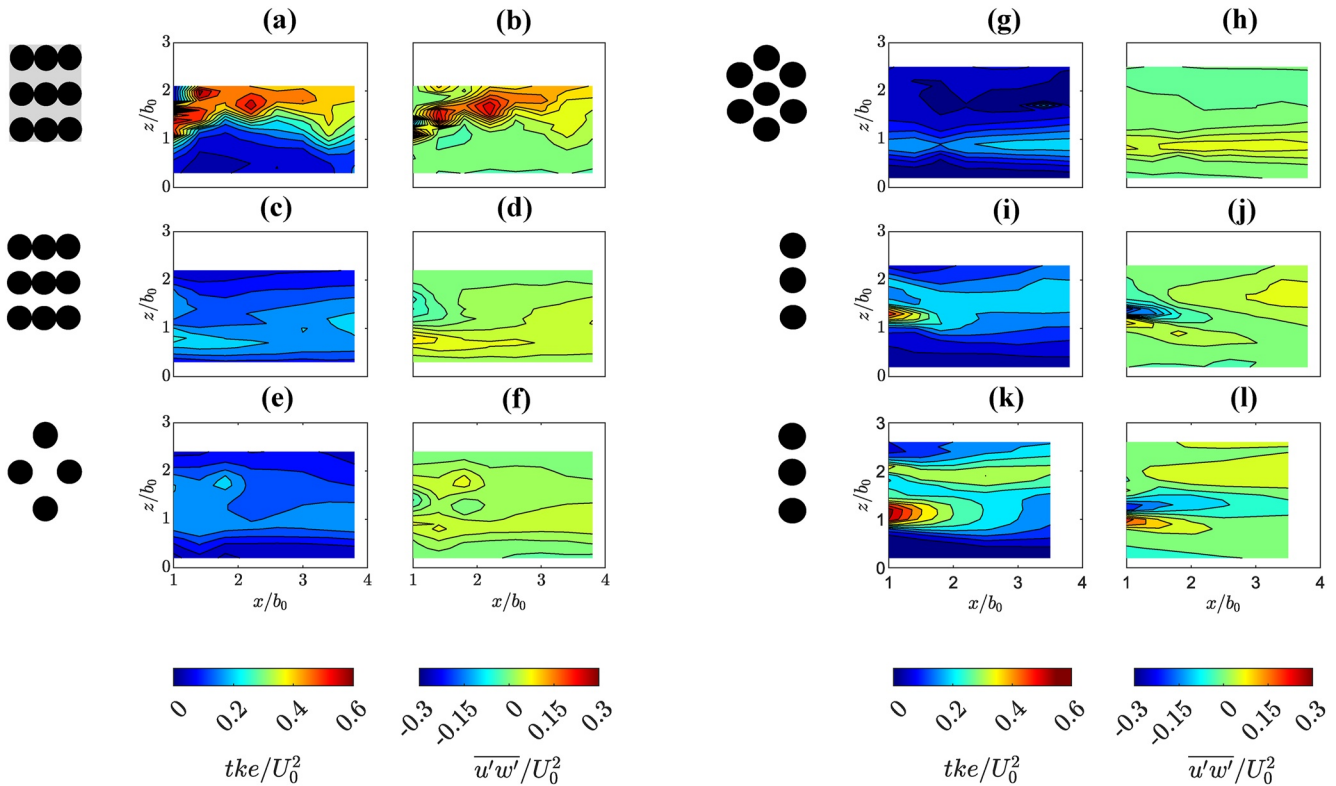


Figure 7. Contours showing turbulent kinetic energy (tke/U_0^2) and vertical Reynolds shear stress ($\overline{u'w'}/U_0^2$) normalized by bulk velocity squared U_0^2 along the main channel centerline (x - z plane) downstream of all logjams; S1 [a, b], S2 [c, d], S3 [e, f], S4 [g, h], S5 [i, j], and S6 [k, l]. Only half of the logjam structures S1 to S4 is shown on the left hand side of the contour plot to indicate their vertical location.

in sign of \overline{w}/U_0 (Figures 6d, 6f, and 6h) immediately downstream of the logjam ($x/b_0 = 1$). The upper wake region of these logjams (S2-4) was characterized by low values of \overline{u}/U_0 (Figures 6c, 6e, and 6g) and tke/U_0^2 (Figures 7d, 7f, and 7h) as indicated by the blue contour colors.

The upper wake region of the short porous logjams (S5-6) was characterized by the presence and decay of the secondary jets and flow diversion between individual logs, shown by the large values \overline{u}/U_0 at the height of the lowest inter-log gap ($1.5 \leq z/b_0 \leq 1.75$) at $x/b_0 = 1$ (Figures 6i and 6k). In comparison to S5, values \overline{u}/U_0 were 1.6 times higher while the maximum tke/U_0^2 was 0.74 times lower for the scaled logjam S6 at height of the lowest inter-log gap. A less distinct secondary jet of lower \overline{u}/U_0 was observed for S2 following the lowest log gap [$x/b_0 = 1$; $z/b_0 = 1.5$; $\overline{u}/U_0 = 0.5$] associated with the increase in streamwise structure length ($L_s(S5) = 1/8 L_s(S2)$).

In the case of the non-porous logjam (S1), the rapid vertical expansion of the lower jet into the upper wake region ($z/b_0 > 1$; $\overline{w}/U_0 \gg 0$, Figure 6b) was associated with greater values $\langle \overline{w} \rangle / U_0$ compared to all long, porous logjams ($x/b_0 = 1$, $\langle \overline{w} \rangle / U_0$, S1: 0.47, S2: -0.04, S3: -0.03, S4: -0.01). This region started at the height of the logjam lower edge ($z/b_0 \approx 1$), showing the highest values in $\overline{u'w'}/U_0^2$ and tke/U_0^2 ($x/b_0 = 1$; $z/b_0 = 1.1$, $(\overline{u'w'}/U_0^2)_{\max} = 0.28$; $z/b_0 = 1.4$, $(tke/U_0^2)_{\max} = 0.61$; Figures 7a and 7b) and progressed upward with increasing streamwise distance from the logjam.

3.2.2. Far Wake Region

3.2.2.1. Recovery of Mean Streamwise Velocity

To analyze the impact of physical logjam design on wake recovery, the velocity deficit ($\Delta\overline{u}$) between the furthest upstream (S1-5: $x/b_0 = -60.2$; S6: $x/b_0 = -30$) and selected downstream profiles were computed for all logjams and is presented in Figures 8a-8f. Values of $\Delta\overline{u} < 0$ indicate that the streamwise velocities measured downstream

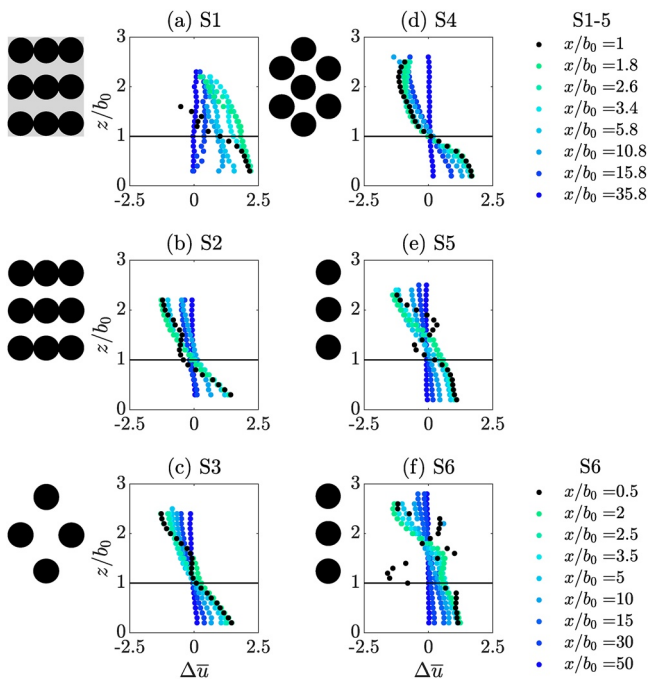


Figure 8. Progression of velocity deficit computed from the difference between furthest upstream profile (S1-5: $x/b_0 = -60.2$; S6: $x/b_0 = -30$) and selected downstream profiles (S1-5: $\Delta\bar{u} = \frac{\bar{u} - \bar{u}_{x/b_0 = -60.2}}{\bar{u}_{x/b_0 = -60.2}}$, S6: $\Delta\bar{u} = \frac{\bar{u} - \bar{u}_{x/b_0 = -30}}{\bar{u}_{x/b_0 = -30}}$). Only half of the logjam structures S1 to S4 are shown on the left hand side of the contour plot to indicate their vertical location. Vertical extent of recorded velocity profiles may vary due to longitudinal changes in downstream flow depth.

of the logjam are smaller than the velocities measured at the furthest upstream profile, resulting in a velocity deficit, while values of $\Delta\bar{u} > 0$ indicate that there are higher mean streamwise velocity values downstream of the logjam than at the unperturbed upstream profile and hence, a velocity surplus.

In the case of the non-porous logjam (S1; Figure 8a), a velocity surplus ($\Delta\bar{u} > 0$) was initially present immediately downstream of the logjam ($x/b_0 = 1$) over $0 \leq z/b_0 \leq 1$ (Figure 8a, black solid circles) and was observed throughout the profile vertical extent for $x/b_0 > 1.4$, which was associated with a rapid vertical expansion of the primary jet and its mixing with the wake and overtopping flow. Similarly, all porous logjams (S4–S6; Figures 8b–8f) initially showed velocity surplus within the lower wake region ($0 \leq z/b_0 \leq 1$) as a result of the high momentum flow exiting beneath the logjams. In the upper wake region ($z/b_0 \approx 1-2.5$), however, a velocity deficit was observed due to low streamwise mean velocities (Figures 6c, 6e, 6g, 6i, and 6k). Close to the logjam structure ($x/b_0 = 1$), both short porous logjams showed additional peaks of velocity surplus due to flow diversion around the individual logs at height of the lowest log gap (Figures 8e and 8f), black solid circles, $z/b_0 \approx 1.7$ and 1.6 for S5 and S6, respectively). These secondary jets, however, diminished by approximately eight times the inter-log gap width ($x/b > 8$) for both logjams as they were dissipated from mixing with the surrounding flow. The depth-average velocity deficit $\Delta\bar{u}$ between the furthest upstream and downstream profiles (Figure 8, blue solid circles) was less than 10% with a maximum absolute magnitude of $\Delta\bar{u}$ less than 20% for all structures. Increasing the scale of S5 resulted in 1.4 times longer wake recovery for the larger-scale logjam S6 which recovered by $x/b_0 \geq 50$.

3.2.2.2. Decay of Maximum Jet Velocity

While the maximum streamwise velocity \bar{u}_{max} and velocity profile $\bar{u}(z)$ of flow exiting the lower gap varied with logjam design, for all logjams, $\bar{u}(z)$ decayed in a self-similar fashion with increasing longitudinal distance from the logjam ($\frac{x}{b_0}$). Decay of local maximum velocity in the lower gap region ($0 < \frac{z}{b_0} < 1$), \bar{u}_{max} , relative to depth-averaged velocity over the lower gap region at the initial downstream measurement point (\bar{u}_{b_0}) with increasing downstream longitudinal distance from the logjam ($\frac{x}{b_0}$)^{-1/2} is shown in Figure 9. Maximum mean streamwise velocity downstream of all structures initially maintained an elevated value close to that obtained at the measurement point nearest to the logjam ($\frac{x}{b_0} = 1$), which was reduced as the mixing region between the jet and surrounding flow reached the location of jet maximum velocity. Measured velocity ratios were within 1.05–1.18 for S1, S3-6 ($\frac{\bar{u}_{max}}{\bar{u}_{b_0}} = 1.14 \pm 0.02, 1.63 \pm 0.03, 1.05 \pm 0.02, 1.16 \pm 0.03, 1.18 \pm 0.01, 1.10 \pm 0.02$, mean $\pm \sigma$ for S1 to S6 over $0 \leq x/b_0 \leq 4$) and above this range for S2 ($\frac{\bar{u}_{max}}{\bar{u}_{b_0}} = 1.63 \pm 0.03$), for which the magnitude of \bar{u}_{max} was greater than the depth-average velocity in the gap region due to a pronounced linear shape of the downstream velocity profile, with maximum observed \bar{u}/U_0 located at the lowest measurement point, $z/b_0 = 0.02$ (Figure 6c).

Both the initial depth-averaged velocity in the lower gap region and the initial maximum jet velocity were increased for logjams with the lowest inverse of the relative channel void area A_{rv}^{-1} (Table 1). S1 and S4 had lower $A_{rv}^{-1} = 0.33$ due to the higher projected area of these structures which occupied the full structure extent, in comparison to S2, S3, S5, and S6 which A_{rv}^{-1} was increased ($A_{rv}^{-1} = 0.43 - 0.5$, Table 1) due to the arrangement of gaps between the structure logs. The average local maximum velocity over $0 \leq x/b_0 \leq 4$ relative to bulk velocity $\frac{\langle \bar{u}_{max} \rangle}{U_0} = 2.9, 2.2, 2.0, 2.5, 1.9, 2.0$ for logjams S1–6, respectively. Downstream of the potential core region ($x/b_0 > 4$), the local maximum jet velocity, \bar{u}_{max} , reduced from the initial value as it lost momentum due to mixing with surrounding flow. The decay of $\frac{\bar{u}_{max}}{\langle \bar{u}_{b_0} \rangle}$ in the region downstream of the potential core scaled with $(x/b_0)^{-1/2}$. Average $C_{wj} \left(\frac{\bar{u}_{max}}{\langle \bar{u}_{b_0} \rangle} \sim C_{wj} (x/b_0)^{-1/2} \right)$ across all structures for $\frac{x}{b_0} > 4$ was $C_{wj} = 3.0 \pm 0.5$ (mean ± 1 standard devi-

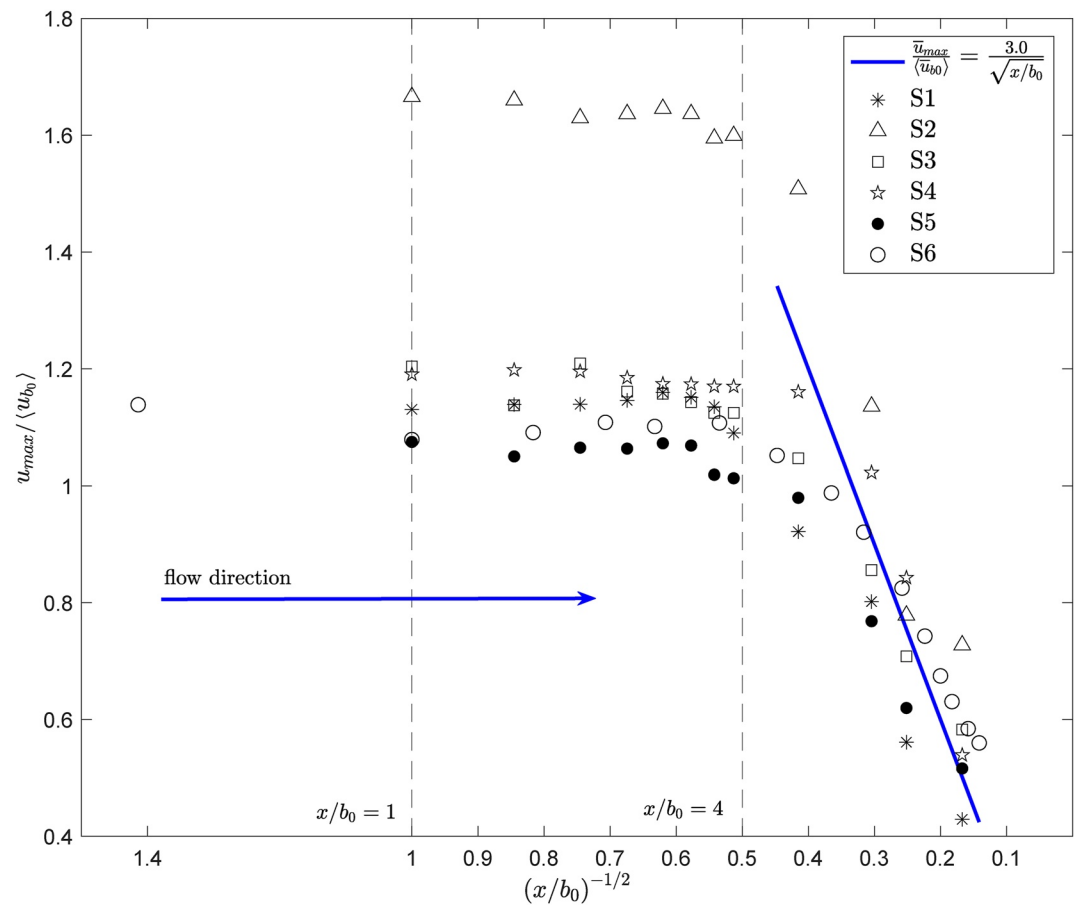


Figure 9. (a) Decay of local maximum velocity \bar{u}_{max} downstream of structures S1-6 relative to depth-averaged initial jet velocity $\langle \bar{u}_{b0} \rangle$ ($0 \leq z/b_0 \leq 1$) with increasing longitudinal distance from the logjam $\left(\frac{x}{b_0}\right)^{-1/2}$, with measurements for S1-6, respectively, represented by black asterisks (S1), open triangles (S2), open squares (S3), open stars (S4), solid circles (S5), and open circles (S6). Dashed black line at $(x/b_0)^{-1/2} = 0.5$ ($x/b_0 = 4$) denotes an observed length of the potential core region over which maximum jet velocity remained close to the initial measured value. Solid blue line indicates observed scaling of longitudinal decay $\left(\frac{\bar{u}_{max}}{\langle \bar{u}_{b0} \rangle} \sim C_{wj}(x/b_0)^{-1/2}$, Wu & Rajaratnam, 1995), with decay coefficient $C_{wj} = 3.0 \pm 0.5$ fit to measurements for S1-6 ($x/b_0 > 4$).

ation of six logjams), with $C_{wj} = 2.4 \pm 0.2$, 3.7 ± 0.5 , 2.6 ± 0.3 , 2.9 ± 0.4 , 3.2 ± 0.3 , 3.2 ± 0.5 respectively for S1-6 (Figure 9, solid blue line; $F_0 \cong 0.5 - 1$).

4. Discussion

4.1. Impact of Engineered Logjam Structures on Channel Hydrodynamics

4.1.1. Hydrodynamic and Hydraulic Changes Associated With Engineered Logjams

A change in the water surface profile and an increase in backwater rise (ΔH) was observed upstream of all logjams. The change in the water surface profile was greater for logjams with a higher frontal projected area (A_p , Table 1). Upstream flow depth increased with proximity to the logjam, causing the flow to spill onto the floodplains. Larger floodplain inundation was observed for logjams with higher cross-sectional blockage (Muhawenimana et al., 2020). The relationship between logjam cross-sectional area and the floodplain water level is a key feature of using channel-spanning ELJs to mitigate flood risk. The subsequent reconnection of the main channel with its adjacent floodplains enhances infiltration into the ground (Burgess-Gamble et al., 2018; Dadson et al., 2017). Hence, an increase in channel obstruction (e.g., through an increase in cross-sectional blockage) will improve flood attenuation (Burgess-Gamble et al., 2018; Dadson et al., 2017; Muhawenimana et al., 2020). Besides the

cross-sectional blockage area of logjams, the backwater rise of logjams without a vertical gap is dependent on the approach flow Froude number, the compactness of the structure, and the percentage of organic fine material such as branches and leaves (Schalko et al., 2018) and can be predicted from the unobstructed flow depth, unit discharge and a dimensionless structural parameter including logjam length, frontal area density, drag coefficient, and solid volume fraction (Follett & Wilson, 2020). Experiments investigating logjams featuring a vertical gap, as in our study, showed that the backwater rise increases with jam resistance and a decrease of the gap height (b_0), and can be predicted using a combination of a sluice gate model and incorporating the hydrodynamic drag generated by the logjam (Follett et al., 2021).

Upstream of all tested logjams, streamwise mean velocities increased near $x/H_s \approx 1$, marking the onset of longitudinal flow diversion (Figure 3). In line with our observation, the onset of longitudinal flow diversion for the flow around porous structures (e.g., submerged vegetated canopies, often represented by vertical wooden logs), was found at a similar streamwise location (Coceal & Belcher, 2004; Rominger & Nepf, 2011). Upstream of the structures, maximum vertical velocity (w) was found close to the lower vertical edge of the lowest log in the structures, with a relative increase in w highest for the non-porous logjam S1. The location and extent of increase in upstream w may assist in understanding the effect of logjams on aquatic organisms and in estimating the onset of longitudinal scour.

Following the flow diversion upstream at height of the main gap ($z/b_0 \leq 1$), a high-momentum jet underneath the structures formed for all logjams (Figure 6), similar to a modified wall jet (Ead & Rajaratnam, 2002) or the flow beneath an engineered or naturally formed logjam (Beebe, 2000). The initial local maximum jet velocity was maintained over a potential core region, extending from $0 \leq \frac{x}{b_0} \leq 4$ (Figure 9, dashed black line at $\frac{x}{b_0} = 4$ associated with a change in curvature for all data series), similar to values previously observed for offset jets with an initial uniform velocity on a rough bed and free jets ($x = 4b_0$, Bhuiyan et al., 2011) but reduced from plane wall jets ($x = 8b_0$, Albayrak et al., 2008). For classic jet flows with an initial near-uniform velocity, the initial local maximum velocity is equal to the uniform jet velocity ($\frac{\bar{u}_{max}}{\langle \bar{u}_{b0} \rangle} = 1$). Measurements conducted in this study yielded $\frac{\bar{u}_{max}}{\langle \bar{u}_{b0} \rangle} > 1$, due to non-uniformity of the initial jet shape and discrete measurement locations. This high-momentum flow presents a key feature for ELJ design to prevent blockage of the logjam main gap by brush and debris, allowing constant base flow and fish movement.

In contrast, the upper wake was structure-dependent ($z/b_0 \geq 1$), strongly depending on log arrangement and longitudinal logjam length. For instance, the upper wake of all long, porous logjams (S2-4) was characterized by low values of \bar{u}/U_0 and tke/U_0^2 (Figures 6 and 7) because of the internal flow diversion slowing the flow through the structures. A similar reduction in mean streamwise velocity was observed for flow around patches of vertical wooden cylinders mimicking submerged vegetated canopies (Zong & Nepf, 2011). Also, the distribution of high shear stresses for these logjams was characterized by mostly positive values at $z/b_0 = 1$, likely originating from the turbulent flow coming from underneath the logjams entraining into the wake region without the development of vortex shedding.

In contrast, the near wake of the short, porous logjam structures (S5-S6) was characterized by the presence and decay of secondary jets due to the presence of distinct flow paths, indicated by the increase in \bar{u}/U_0 at height of the inter-log gaps (b) (Figure 6). For these logjams, regions of high vertical Reynolds shear stress were found downstream of the lowest log (Figure 7), with $\overline{u'w'}/U_0^2 > 0$, indicating turbulent momentum in the upward direction, and values of negative $\overline{u'w'}/U_0^2$ distributed mostly at the upper edge of the lowest log, indicating turbulent momentum transport downward. This pattern is similar to that in a cylinder wake with vortex shedding (Ouro et al., 2019; Williamson, 1996), suggesting that this transient phenomenon also takes place for S5 and S6. In contrast, weaker secondary jets were observed for the longer, porous logjam S2.

Furthermore, the upper wake of the non-porous logjam (S1) was characterized by the expansion of the high-momentum jet into the upper wake region, resulting in a large velocity gradient which increases Reynolds shear stress. Similar, downstream flow alterations were observed for flow exiting an under-shot sluice gate, not only showing the expansion of the high momentum flow but indicating the existence of a recirculation zone at structure height (Ead & Rajaratnam, 2002). Due to the physical limitations of the ADV, the existence of such a recirculation zone could not be proven.

Wake recovery was self-similar (Figure 9; Bhuiyan et al., 2011), independent of the physical logjam design, and scale with $(x/b_0)^{-1/2}$, similar to previous observations for plane free jets ($\frac{\bar{u}_{max}}{\langle \bar{u}_{b0} \rangle} \sim (x/b_0)^{-1/2}$, Rajaratnam, 1976) and plane wall jets ($\frac{\bar{u}_{max}}{\langle \bar{u}_{b0} \rangle} \sim C_{wj}(x/b_0)^{-1/2}$; Albayrak et al., 2008; Barenblatt et al., 2005; Bhuiyan et al., 2011; Wu & Rajaratnam, 1995). The decay occurred over an elongated length scale for wall jets relative to free jets due to reduced entrainment, with the decay coefficient C_{wj} observed to be related to jet Froude number, $F_0 = \langle \bar{u}_{b0} \rangle / \sqrt{gb_0}$ ($C_{wj} \sim 3.5$, $F_0 = 3 - 9$; Wu & Rajaratnam, 1995; $C_{wj} \sim 2.7$, $F_0 \cong 1$, Albayrak et al., 2008). An average decay coefficient $C_{wj} = 3.0 \pm 0.5$ was observed for all logjam designs, with $F_0 = 0.78 \pm 0.16$. Wake decay was almost complete by $x/b_0 \geq 35$ for logjams S1–5 and by $x/b_0 = 50$ for S6. The wake length decay scale is of interest when introducing multiple logjams along a stream. For example, allowing the full decay distance between logjams allows the decay of logjam-induced increases in maximum longitudinal velocity and turbulence, promoting suspended sediment capture.

4.1.2. Scaling Impacts

Scaling impacts were examined through a generalized 1:2 scale test (S6) of the short, porous logjam S5. We acknowledge that the comparison of our results for S5 and S6 is limited by the absence of floodplains in the S6 test case. Results showed that a similar near wake structure was generated by both structures, with a main secondary jet generated in the gap between the lower and middle logs (Figures 6 and 7). For all structures including S5 and S6, the region over which maximum jet velocity remained close to the initial measured value extended four gap widths downstream (Figure 9; Abramovich & Schindel, 1963). Although the difference was slight between all structures, Froude scaling of bulk velocity resulted in similar jet Froude numbers for both structures ($F_0 = 3.18$, 3.21 for S5, S6, respectively) and similar magnitude of wall jet coefficient, ($C_{wj} = 3.2 \pm 0.3$, 3.2 ± 0.5 for S5, S6, respectively), which was previously observed to vary with jet Froude number (Albayrak et al., 2008; Wu & Rajaratnam, 1995). However, the long-distance recovery of the primary jet was found to require a slightly longer relative distance in the larger scale S6, for which the wake recovery distance, relative to gap width, was 1.4 times longer than the smaller scale S5 (Figure 8).

4.1.3. Study Limitations

We acknowledge that the transferability and comparability of our results to real-life logjams are limited. First, logjams installed in the field will not consist of idealized horizontal cylinders equally spaced and of identical size, but rather of non-uniform logs sourced from the adjacent floodplains, consisting of varying diameter, roughness, and curvature. Using natural materials (e.g., twigs, logs) or 3D-printed representations of wood can increase logjam complexity, mimicking more closely the characteristics of natural ELJs while maintaining the controllability of logjam properties (Friedrich et al., 2021). Second, logjam structure is subject to changes in shape, log arrangement, and void ratio caused by the accumulation of fine organic material and its decay (Schalko et al., 2018). These changes result in continuous changes in the near wake and hence, further research is required to quantify the impact of such changes on channel hydrodynamics. Third, all experiments were conducted using a non-mobile smooth bed which may have increased the near-bed streamwise velocities and neglected the interaction between logjam, flow, and sediment transport processes (Schalko et al., 2021). This is an important relationship that requires further experimental investigation (Friedrich et al., 2021) as, for instance, the use of a movable bed was found to decrease backwater rise associated with channel-spanning logjams (Schalko et al., 2019a). Furthermore, experiments were only conducted under bankfull flow conditions. Hence, further research is required to quantify the impact of ELJ design on channel hydrodynamics under varying flow conditions. While Müller et al. (2021b) showed similar upstream and downstream hydrodynamic changes under 80% bankfull discharge, lower and higher flow depths may change turbulent structures and channel-floodplain interactions. Finally, the physical limitations of the ADV (i.e., submergence of the ADV head and required distance from the logjam) prevented velocity measurements over the upper part of the water column and within approximately 50 mm upstream and downstream of the logjam. The interaction between overtopping flow and the near wake is an important aspect as an experimental study of a submerged log showed that overtopping flow can inhibit the formation of turbulent structures (Schalko et al., 2021), and therefore would significantly influence the near wake. Thus, a research gap remains to characterize the impact of overtopping flow on the near wake and turbulent structures generated immediately downstream of the logjam. High-fidelity simulations and advanced velocity

measurement techniques (e.g., PIV) may be advantageous to unveil the instantaneous flow in such a region. Nevertheless, our results highlight important flow alterations that are a result of logjam structure and scaling.

4.2. Anticipated Impacts of Hydrodynamic Changes Associated With Engineered Logjams on the Aquatic Environment

Our upstream and downstream hydrodynamic measurements showed a range of hydrodynamic changes due to logjam installation which may have both advantageous and detrimental effects on the aquatic environment, including channel geomorphology and aquatic ecology. In the following section, the anticipated impacts of ELJs on the aquatic environment are discussed and further research needs are highlighted.

4.2.1. Impacts on Channel Geomorphology

Upstream vertical flow diversion and the resulting high-momentum flow beneath all logjams (Figure 6) are presumed to elevate bed shear stress, and therefore, to increase the risk of pit formation and particle mobilization if the maximum jet velocity underneath the logjams exceeds the critical Shields parameter. Scour formation is anticipated to coincide with the onset of upstream flow diversion ($x/H_s \approx 1$) and to be the largest within the region in which the initial jet core is being preserved ($x/b_0 \leq 4$) for all logjams (Figure 9). Alongside engineered logjams (Follett et al., 2021; Follett & Wilson, 2020), similar scour formations have been observed for flow underneath sluice gates (Uyumaz, 1988), in-stream wood (Wallerstein & Thorne, 2004), accumulation of wooden pieces on retention racks (Al-Zawaidah et al., 2021; Schalko et al., 2019b) and bridge piers (Lagasse et al., 2010). Scour formation and extent were found to depend on discharge and structure properties. While Schalko et al. (2019b) showed that scour depth increased with discharge for wood accumulations at vertical retention racks, Lagasse et al. (2010) identified size, shape, and location of logjams as key parameters influencing scour associated with wood accumulations at bridge piers. In contrast, logjam roughness and porosity were found to not significantly impact scour pattern and depth (Lagasse et al., 2010). A study analyzing wood accumulation at a vertical retention rack showed that wood accumulations forming near the water surface (i.e., triangular distribution shape) caused deep bed to scour which extended in a longitudinal direction but less downstream sediment deposition (Al-Zawaidah et al., 2021). As ELJs used for natural flood management span the width of the channel, they are likely to accumulate organic material which reduces logjam void ratio and therefore, increases scour formation and extent. Furthermore, scour was found to increase with an increase in cross-sectional blockage area due to the increase in flow diversion (Beebe, 2000; Lagasse et al., 2010). These observations indicate that the largest scour may be expected for our non-porous logjam (S1) which also showed the highest primary jet velocity. Based on the variety of engineered logjam characteristics, which may influence the extend of scour, there is a need for further experimental studies.

An increase in the likelihood of bedload transport is expected due to the high streamwise velocity and bed shear stress observed in the region of the primary jet, which increases the Shields number (Julien, 2010). This, in turn, is likely to increase the flushing of gravel and fine sediment underneath the structure, enhancing habitat quality through the creation of suitable spawning habitat (Boulton, 2007). In addition, an increase in Reynolds stress and turbulent kinetic energy was observed in the near wake region downstream of the non-porous (S1) and short, porous (S5-6) ELJ (Figure 7), which would increase the mixing of suspended sediment (Julien, 2010). Moreover, the flushing of fine sediment from bed material may also promote hyporheic exchange and therefore an increase in dissolved oxygen within the hyporheic zone, beneficial for aquatic organisms (e.g., salmonids) (Boulton, 2007). Yet, there remains a research gap in quantifying the interaction between the primary jet and hyporheic exchange.

The high-momentum flow observed for all logjams may also result in bank erosion within the gap between logjam structure and bed (Figure 6), potentially influencing the structural integrity. Flume studies examining partially channel-spanning emergent side logs showed that a single log can increase the potential of bank erosion due to flow diversion toward the gap between log and bank, almost doubling near bank velocities (Zhang et al., 2020a) while the introduction of multiple logs in the longitudinal direction reduced erosion rates because of the wake interference between logs (Zhang et al., 2020b). Gap width was found to be a key parameter influencing near bank velocities and therefore bank erosion (Zhang et al., 2020a) which is comparable to the gap between the flume bed and logjam lower edge in this study. Following these observations, further research is required to examine the impact of the observed primary jet on the bed and bank erosion in relation to b_0 . To prevent ELJs from structural failures, key logjam members should be restrained using anchors, wooden posts, ropes, and ballast (Association

of Directors of Environment, Economy, Planning and Transport, 2019; Shields & Alonso, 2012) and a log length more than twice the channel width is recommended for ELJs construction to reduce log mobility (Association of Directors of Environment, Economy, Planning and Transport, 2019). Further research investigating lift and drag forces acting on the logjam structure may be beneficial to estimate structural resistance under varying flow conditions as unsteady flow conditions were found to increase forces by about two to three times compared to steady flow conditions (Shields & Alonso, 2012).

4.2.2. Ecological Impacts and Prospects

While the wide range of flow alterations observed in our study is expected to enhance habitat complexity and therefore, result in an increase in fish habitat diversity (Dolloff & Warren, 2003; Wallerstein & Thorne, 2004), certain flow alterations, such as the formation of the primary jet (Figure 6), may present velocity barriers to fish. While strong swimming species (e.g., salmonids) were not prevented from passing into the upstream region when exposed to a subset of the investigated logjam configurations (Müller et al., 2021b), weaker swimming species and juveniles may struggle to overcome the high streamwise velocities. Furthermore, repeated exposure to regions of high-momentum flow due to the installation of multiple ELJs along a river stretch may result in an increase in energy expenditure and delay fish movement or prevent fish from reaching certain habitats. Further research is required to quantify the cumulative impacts of multiple ELJs on catchment hydrodynamics and care should be taken in selecting a physical design to maintain habitat connectivity for all species present in the corresponding river.

Besides the impact of the primary jet on fish movement, a research gap remains in quantifying the impact, if any, of the structure-dependent upper near wake ($z/b_0 \geq 1$). The increased turbulence associated with the non-porous (S1) and the short porous logjams (S5-6) as well as along the shear layer between upper wake and primary jet (Figure 7), may act as a deterrent as fish have been found to avoid regions of high turbulent kinetic energy, Reynolds shear stresses, and coherent vertical structures (Hockley et al., 2014; Muhawenimana et al., 2019; Tritico & Cotel, 2010). In contrast, the reduced mean velocities and turbulence level in the case of the long, porous logjams (S2-4; Figures 6 and 7) may provide resting and foraging areas for fish.

Engineered logjams may also contribute to river restoration. Under higher flow conditions, logjams can create seasonal wetlands by reconnecting the main channel with its floodplains (Table 1; Zalewski et al., 2003), supporting lateral habitat connectivity (Burgess et al., 2012), providing fish spawning and nursery grounds (Sheaffer & Nickum, 1986), as well as low velocity areas, protecting fish from downstream displacement during high flows (Franssen et al., 2006). Furthermore, the observed flow alterations will enhance habitat complexity through the creation of scour pools and other bed forms (Fausch & Northcote, 1992). Another important aspect is the creation of cover and refugia for fish (Dolloff & Warren, 2003; Senter & Pasternack, 2011). Hence, the targeted modification of the physical design of ELJs may not only mitigate flood risk but also be used as a tool to adapt habitat suitability depending on the species present (Schalko et al., 2021). Yet, a research gap remains in quantifying the impact of these structures as part of river restoration projects (e.g., habitat enhancement for aquatic organisms).

5. Conclusions

Despite increasing interest in the use of channel-spanning engineered logjams as nature-based solutions for flood risk management, little is known about the impact of physical logjam design on local channel hydrodynamics and associated alterations of the riverine environment. Here, we provide experimental evidence on upstream and downstream changes in channel hydrodynamics of six idealized ELJ structures through ADV measurements and dye visualization. We show that flow was diverted toward the lower gap (b_0) between the bed and logjam's lower edge upstream of these logjams, creating a primary jet whose strength varied with the physical logjam design. Jet local maximum velocities were maintained until a downstream distance of $4b_0$ before rapidly decaying with an average wake decay coefficient of 3.0 ± 0.5 . The upper wake was structure-dependent, featuring smaller secondary jets for all porous logjams with distinct flow paths (S2-3, S5-6), and particularly pronounced for the short logjam structures (S5-6) that resembled flow around cylinders. In fact, increasing logjam void ratio leads to more steady wakes with lower turbulent kinetic energy and shear stress levels. Therefore, near wake decay was dependent on physical design parameters while far wake decay was shown to be self-similar, resulting in almost full flow recovery at downstream distances of $35b_0$ and $50b_0$ for S1-5 and S6, respectively. Our findings provide a better understanding of the impact of physical logjam designs on channel hydrodynamics. Furthermore, the

upstream and downstream hydrodynamic analysis showed the reach length over which hydrodynamic changes extend, providing information on logjam positioning and an estimate of possible changes in channel geomorphology and fish habitat. Our work expands the current state of knowledge on engineered logjams and supports the delivery of these structures as environmentally friendly hydraulic structures used for natural flood management.

Nomenclature

A_p	frontal projected area
A_{rv}	relative channel void area
b	inter-cylinder gap height
b_0	vertical gap height between flume bed and logjam
B_{flume}	flume width
B_{fp}	floodplain width
B_{mc}	main channel width
C_{wj}	jet decay coefficient
d	log diameter
F_0	jet Froude number
Fr	Froude number
g	gravitational constant
H	flow depth
H_{flume}	flume height
H_{mc}	main channel height
H_s	logjam height
$\overline{H_1}$	mean upstream flow depth
$\overline{H_2}$	mean downstream flow depth
ΔH	backwater rise
L_{flume}	flume length
L_s	logjam longitudinal length
n	number of logs
Q	discharge
Re_d	Reynolds number based on log diameter
tke	turbulent kinetic energy
u	streamwise velocity component
\bar{u}	mean streamwise velocity
\bar{u}_{max}	maximum mean streamwise velocity
$\langle \bar{u} \rangle$	depth-average mean streamwise velocity
$\langle \bar{u}_{b_0} \rangle$	depth-average initial jet velocity
$\Delta \bar{u}$	mean streamwise velocity deficit
u'	streamwise velocity fluctuation
$\sqrt{u'^2}$	root mean square velocity fluctuation
$\overline{u'w'}$	vertical Reynolds shear stress
U_0	bulk velocity
v	lateral velocity component
\bar{v}	mean lateral velocity
v'	lateral fluctuation velocity
V_{void}	pore volume
$V_{control}$	volume occupied by non-porous logjam
V_{solid}	volume occupied by solid logjam
w	vertical velocity component
\bar{w}	mean vertical velocity
$\langle \bar{w} \rangle$	depth-average mean vertical velocity
w'	vertical fluctuation velocity
x	longitudinal direction

y	lateral direction
z	vertical direction
Φ	logjam void ratio
ν	kinematic viscosity

Conflict of Interest

The authors declare no conflicts of interest relevant to this study.

Data Availability Statement

Data underpinning the results presented here and a Figure (S1) depicting the measurement locations can be found in the Cardiff University data catalogue: <http://doi.org/10.17035/d.2021.0131419068>.

Acknowledgments

We thank Paul Leach, Steven Rankmore, and Valentine Muhawenimana for technical assistance, and Yin Lok Kwan and Ana Pinto Oliveira for their help in conducting the ADV measurements. The first author was funded as part of the Water Informatics Science and Engineering Center for Doctoral Training (WISE CDT) [EP/L016214/1] from the Engineering and Physical Science Research Council (EPSRC). The second author was funded by the European Union's Horizon 2020 research and innovation program under the Marie Skłodowska-Curie grant agreement WoodJam (745348), the Royal Academy of Engineering's Research Fellowships program (RF/201920/19/311) and the European Regional Development Fund through the Welsh Government Sêr Cymru program (80762-CU-241).

References

- Abbe, T. B., & Montgomery, D. R. (1996). Large woody debris jams, channel hydraulics and habitat formation in large rivers, *Regulated Rivers, Research Management*, 12, 201–221.
- Abramovich, G. N., & Schindel, L. (1963). *The theory of turbulent jets* (p. 684). MIT Press.
- Albayrak, I., Hopfinger, E. J., & Lemmin, U. (2008). Near-field flow structure of a confined wall jet on flat and concave rough walls. *Journal of Fluid Mechanics*, 606, 27–49. <https://doi.org/10.1017/s0022112008001444>
- Al-Zawaidah, H., Ravazzolo, D., & Friedrich, H. (2021). Local geomorphic effects in the presence of accumulations of different densities. *Geomorphology*, 389, 107838. <https://doi.org/10.1016/j.geomorph.2021.107838>
- Association of Directors of Environment, Economy, Planning and Transport. (2019). Assessing the potential hazards of using leaky woody structures for natural flood management, technical report.
- Barenblatt, G. I., Chorin, A. J., & Prostokishin, V. M. (2005). The turbulent wall jet: A triple-layered structure and incomplete similarity. *Proceedings of the National Academy of Science, USA*, 102(25), 8850–8853. <https://doi.org/10.1073/pnas.0503186102>
- Beebe, J. T. (2000). Flume studies of the effect of perpendicular log obstruction on flow patterns and bed topography. *Great Lakes Geographer*, 7(1), 9–25.
- Bennett, S. J., Ghaneizad, S. M., Gallisdorfer, M. S., Cai, D., Atkinson, J. F., Simon, A., & Langendoen, E. J. (2015). Flow, turbulence, and drag associated with engineered log jams in a fixed-bed experimental channel. *Geomorphology*, 248, 172–184. <https://doi.org/10.1016/j.geomorph.2015.07.046>
- Bhuiyan, F., Habibzadeh, A., Rajaratnam, F., & Zhu, D. Z. (2011). Reattached turbulent submerged offset jets on rough beds with shallow tailwater. *Journal of Hydraulic Engineering*, 137(12), 1636–1648. [https://doi.org/10.1061/\(ASCE\)HY.1943-7900.0000462](https://doi.org/10.1061/(ASCE)HY.1943-7900.0000462)
- Bisson, P. A., Wondzell, S. M., Reeves, G. H., & Gregory, S. V. (2003). Trends in using wood to restore aquatic habitats and fish communities in Western North American rivers. In S. V. Gregory, K. L. Boyer, & A. M. Gurnell (Eds.) (Vol. 37, pp. 391–406), *The ecology and management of wood in world rivers*. American Fisheries Society Symposium.
- Boulton, A. J. (2007). Hyporheic rehabilitation in rivers: Restoring vertical connectivity. *Freshwater Biology*, 52(4), 632–650. <https://doi.org/10.1111/j.1365-2427.2006.01710.x>
- Burgess, O. T., Pine, W. E., III, & Walsh, S. J. (2012). Importance of floodplain connectivity to fish populations in the Apalachicola river, Florida. *River Research and Applications*, 29(6), 718–733. <https://doi.org/10.1002/rra.2567>
- Burgess-Gamble, L., Ngai, R., Wilkinson, M., Nisbet, T., Pontee, N., Harvey, R., et al. (2018). *Working with natural processes – evidence directory*. Environmental Agency. project number: SC150005.
- Coccal, O., & Belcher, S. E. (2004). A canopy model of mean winds through urban areas. *Quarterly Journal of the Royal Meteorological Society*, 130(599), 1349–1372. <https://doi.org/10.1256/qj.03.40>
- Dadson, S. J., Hall, J. W., Murgatroyd, A., Acreman, M., Bates, P., Beven, K., et al. (2017). A restatement of the natural science evidence concerning catchment-based 'natural' flood management in the UK. *Proceedings of the Royal Society A*, 473(2199), 473. <https://doi.org/10.1098/rspa.2016.0706>
- Daubner, T., Kizhofer, J., & Dinulescu, M. (2018). Experimental investigation of five parallel plane jets with variation of Reynolds number and outlet conditions. *EPJ Web of Conferences*, 180, 1–8. <https://doi.org/10.1051/epjconf/201818002018>
- Dodd, J. A., Newton, M., & Adams, C. E. (2016). *The effect of natural flood management in-stream wood placements on fish movement in Scotland*. CREW Scotland's Centre of Expertise for Water.
- Dolloff, C. A., & Warren, M. L., Jr. (2003). Fish relationships with large wood in small streams. *American Fisheries Society Symposium*, 37, 179–193.
- Ead, S. A., & Rajaratnam, N. (2002). Plane turbulent wall jets in shallow tailwater. *Journal of Engineering Mechanics*, 128, 143–155. [https://doi.org/10.1061/\(ASCE\)0733-9399~20021128:2\(143\)](https://doi.org/10.1061/(ASCE)0733-9399~20021128:2(143))
- Estrela, T., Menedez, M., Dimas, M., Marcuello, C., Rees, G., Weber, K., et al. (2001). Sustainable water use in Europe, Part 3: Extreme hydrological events: Floods and draughts.
- Fausch, K. D., & Northcote, T. G. (1992). Large woody debris and salmonid habitat in a small coastal British Columbia stream. *Canadian Journal of Fisheries and Aquatic Sciences*, 49(4), 682–693. <https://doi.org/10.1139/f92-077>
- Follett, E., Schalko, I., & Nepf, H. (2020). Momentum and energy predict the backwater rise generated by a large wood jam. *Geophysical Research Letters*, 47(17), e2020GL089346. <https://doi.org/10.1029/2020GL089346>
- Follett, E., Schalko, I., & Nepf, H. (2021). Logjams with a lower gap: Backwater rise and flow distribution beneath and through logjam predicted by two-box momentum balance. *Geophysical Research Letters*, 48(16), e2021GL094279. <https://doi.org/10.1029/2021GL094279>
- Follett, E. M., & Wilson, C. A. M. E. (2020). Bedload sediment transport induced by channel-spanning instream structures. In *River flow 2020*. In *Proceedings of the 10th Conference on Fluvial Hydraulics*. <https://doi.org/10.1201/b22619-104>
- Forest Research. (2007). The Robin wood flood report: Evaluation of large woody debris in watercourses.

- Franssen, N. R., Gido, K. B., Guy, C. S., Tripe, J. A., Shrank, S. J., Strakosh, T. R., et al. (2006). Effects of floods on fish assemblages in an intermittent prairie stream. *Freshwater Biology*, 51(11), 2072–2086. <https://doi.org/10.1111/j.1365-2427.2006.01640.x>
- Friedrich, H., Ravazzolo, D., Ruiz-Villanueva, V., Schalko, I., Spreitzer, G., Tunncliffe, J., & Weitbrecht, V. (2021). Physical modelling of large wood (LW) processes relevant for river management: Perspectives from New Zealand and Switzerland. *Earth Surface Processes and Landforms*, 1–26. <https://doi.org/10.1002/esp.5181>
- Fujisawa, N., Nakamura, K., & Srinivas, K. (2004). Interaction of two parallel plane jets of different velocities. *Journal of Visualization*, 7(2), 135–142. <https://doi.org/10.1007/bf03181586>
- Gallisdorfer, M. S., Bennett, S. J., Atkinson, J. F., Ghaneizad, S. M., Brooks, A., Simon, A., & Langendoen, E. J. (2014). Physical-scale model designs for engineered log jams in rivers. *Journal of Hydro-environment Research*, 8(2), 115–128. <https://doi.org/10.1016/j.jher.2013.10.002>
- Goring, D. G., & Nikora, I. V. (2002). Despiking acoustic Doppler velocimeter data. *Journal of Hydraulic Engineering*, 128(1), 117–126. [https://doi.org/10.1061/\(ASCE\)0733-9429\(2002\)128:1\(117\)](https://doi.org/10.1061/(ASCE)0733-9429(2002)128:1(117))
- Gregory, S. V., Boyer, K. L., & Gurnell, A. M. (2003). *The ecology and management of wood in world rivers*. American Fisheries Society.
- Hockley, F. A., Wilson, C. A. M. E., Brew, A., & Cable, J. (2014). Fish response to flow velocity and turbulence in relation to size, sex and parasite load. *Journal of The Royal Society Interface*, 11(91), 11. <https://doi.org/10.1098/rsif.2013.0814>
- Jia, G., Shevliakova, E., Eduardo, A. N. P., De Noblet-Ducoudre, N., Richard, H., House, J., et al. (2019). Chapter 2: Land–climate interactions climate change and Land: An IPCC special report on climate change, desertification, land degradation, sustainable land management, food security, and greenhouse gas fluxes in terrestrial ecosystems, final government distribution, technical report.
- Julien, P. Y. (2010). *Erosion and Sedimentation* (2nd ed.). Cambridge University Press.
- Kahraman, A., Ozgoren, M., & Sahin, B. (2012). Flow structure from a horizontal cylinder coincident with a free surface in shallow water flow. *Thermal Science*, 16(1), 93–107. <https://doi.org/10.2298/tsci110719087k>
- Lagasse, P. F., Zevenberger, L. W., & Clopper, P. E. (2010). Impacts of debris on bridge pier scour. In *Scour and erosion, International Conference on scour and erosion*. American Society of Civil Engineers.
- Lam, K., Li, J. Y., Chan, K. T., & So, R. M. C. (2003). Flow pattern and velocity field distribution of cross-flow around four cylinders in a square configuration at a low Reynolds number. *Journal of Fluids Structure*, 17(5), 665–679. [https://doi.org/10.1016/S0889-9746\(03\)00005-7](https://doi.org/10.1016/S0889-9746(03)00005-7)
- Lam, K., & Lo, S. C. (1992). A visualization study of cross-flow around four cylinders in a square configuration. *J. Fluids Struct.*, 6(1), 109–131. [https://doi.org/10.1016/0889-9746\(92\)90058-B](https://doi.org/10.1016/0889-9746(92)90058-B)
- Lam, K., & Zou, L. (2009). Experimental study and large eddy simulation for the turbulent flow around four cylinders in an in-line square configuration. *International Journal of Heat and Fluid Flow*, 30(2), 276–285. <https://doi.org/10.1016/j.ijheatfluidflow.2009.01.005>
- Lehman, J., Coumou, D., & Frieler, K. (2015). Increased record-breaking precipitation events under global warming. *Climate Change*, 32, 501–515. <https://doi.org/10.1007/s10584-015-1434-y>
- Lehmkuhl, O., Rodríguez, I., Borrell, R., & Oliva, A. (2013). Low-frequency unsteadiness in the vortex formation region of a circular cylinder. *Physics of Fluids*, 25(8), 085109. <https://doi.org/10.1063/1.4818641>
- Linstead, C., & Gurnell, A. M. (1999). *Large woody debris in British headwater rivers: Physical habitat role and guidelines*. Technical Report W185, Environment Agency, Rio House.
- Matlab (2018) MATLAB Release 2018b, Natick, Massachusetts: The MathWorks Inc.
- Mori, N. (2020). Despiking. MATLAB Central file exchange.
- Mori, N., Suzuki, T., & Kakuno, S. (2007). Noise of acoustic Doppler velocimeter data in bubbly flow. *Journal of Engineering Mechanics*, 133(1), 122–125. <https://doi.org/10.1061/ASCE0733-93992007133:1122>
- Muhawenimana, V., Wilson, C. A. M. E., Nejjodova, J., & Cable, J. (2020). Flood attenuation hydraulics of channel-spanning leaky barriers. *Journal of Hydrology*, 596, 125731. <https://doi.org/10.1016/j.jhydrol.2020.125731>
- Muhawenimana, V., Wilson, C. A. M. E., Ouro, P., & Cable, J. (2019). Spanwise cylinder wake hydrodynamics and fish behavior. *Water Resources Research*, 55(11), 8569–8582. <https://doi.org/10.1029/2018WR024217>
- Müller, S., Wilson, C., Ouro, P., & Cable, J. (2021a). Experimental investigation of physical leaky barrier design implications on juvenile rainbow trout (*Oncorhynchus mykiss*) movement. *Water Resources Research*, 57(8), e2021WR030111. <https://doi.org/10.1029/2021WR030111>
- Müller, S., Wilson, C., Ouro, P., & Cable, J. (2021b). Leaky barriers: Leaky enough for fish to pass? *Journal of the Royal Society Open Science*, 8(3), 201843. <https://doi.org/10.1098/rsos.201843>
- National Trust. (2015). From source to sea – Natural flood management – The Holnicote experience, project code. *RMP*, 5508.
- Nisbet, T., Roe, P., Marrington, S., Thomas, H., Broadmeadow, S., & Valatin, G. (2015). Defra FCERM Multi-objective flood management demonstration project, project RMP5455: Slowing the flow at Pickering, final report: Phase II.
- Nishino, T., Roberts, G. T., & Zhang, X. (2008). Unsteady RANS and detached-eddy simulations of flow around a circular cylinder in ground effect. *Journal of Fluids and Structures*, 24(1), 18–33. <https://doi.org/10.1016/j.jfluidstructs.2007.06.002>
- Nortek AS. (2009). Vectrino Velocimetry User Guide, Vangkroken, Norway.
- Nortek Support Center. (2019). How do I enhance Correlation and SNR? Retrieved from <https://support.nortekgroup.com/hc/en-us/articles/360029819951-How-do-I-enhance-Correlation-and-SNR->
- Ouro, P., Muhawenimana, V., & Wilson, C. A. M. E. (2019). Asymmetric wake of a horizontal cylinder in close proximity to a solid boundary for Reynolds numbers in the subcritical turbulence regime. *Physical Review Fluids*, 4(10), 104604. <https://doi.org/10.1103/PhysRevFluids.4.104604>
- Rajaratnam, N. (1976). *Turbulent jets*. Elsevier Scientific.
- Reich, M., Kershner, J. L., & Wildman, R. C. (2003). *Restoring streams with large wood: A synthesis*. American Fisheries Society Symposium.
- Rominger, J. T., & Nepf, H. (2011). Flow adjustment and interior flow associated with a rectangular porous obstruction. *Journal of Fluid Dynamics*, 680, 636–659. <https://doi.org/10.1017/jfm.2011.199>
- Santato, S., Bender, S., & Schaller, M. (2013). *The European flood directive and opportunities offered by land use planning*, CSC Report 12. Climate Service Center.
- Schalko, I., Lageder, C., Schmocker, L., Weitbrecht, V., & Boes, R. M. (2019a). Laboratory flume experiments on the formation of spanwise large wood accumulations: I. Effect on backwater rise. *Water Resources Research*, 55(6), 4854–4870. <https://doi.org/10.1029/2018WR024649>
- Schalko, I., Lageder, C., Schmocker, L., Weitbrecht, V., & Boes, R. M. (2019b). Laboratory flume experiments on the formation of spanwise large wood accumulations: Part II – Effect on local scour. *Water Resources Research*, 55(6), 4871–4885. <https://doi.org/10.1029/2018WR024649>
- Schalko, I., Schmocker, L., Weitbrecht, V., & Boes, R. M. (2018). Backwater rise due to large wood accumulation. *Journal of Hydraulic Engineering*, 144(9), 04018056. [https://doi.org/10.1061/\(ASCE\)HY.1943-7900.0001501](https://doi.org/10.1061/(ASCE)HY.1943-7900.0001501)
- Schalko, I., Wohl, E., & Nepf, H. M. (2021). Flow and wake characteristics associated with large wood to inform river restoration. *Scientific Reports*, 11(1), 8644. <https://doi.org/10.1038/s41598-021-87892-7>
- Senter, A. E., & Pasternack, G. B. (2011). Large wood aids spawning chinook salmon (*Oncorhynchus tshawytscha*) in marginal habitat on a regulated river in California. *River Research and Applications*, 27, 550–565. <https://doi.org/10.1002/rra.1388>

- SEPA. (2016). *Natural flood management handbook*. Scottish Environment Protection Agency.
- Sheaffer, W. A., & Nickum, J. G. (1986). Backwater areas as nursery habitats for fishes in pool 13 of the upper Mississippi river. *Hydrobiologia*, 136(1), 131–139. <https://doi.org/10.1007/BF00051510>
- Shields, F. D., Jr., & Alonso, C. V. (2012). Assessment of flow forces on large wood in rivers. *Water Resources Research*, 48(5), W04516. <https://doi.org/10.1029/2011WR011547>
- Strosser, P., Delacámara, G., Hanus, A., Williams, H., & Jaritt, N. (2015). A guide to support the selection, design and implementation of natural water retention measures in Europe – Capturing the multiple benefits of nature-based solutions.
- Tritico, H. M., & Cotel, A. J. (2010). The effect of turbulent eddies on the stability and critical swimming speed of creek chub (*Semotilus atromaculatus*). *Journal of Experimental Biology*, 213(13), 2284–2293. <https://doi.org/10.1242/jeb.041806>
- Woodland Trust, W. (2016). Natural flood management guidance: Woody dams, deflectors and diverters.
- Uyumaz, A. (1988). Scour downstream of a vertical gate. *Journal of Hydraulic Engineering*, 114(7), 811–816. [https://doi.org/10.1061/\(ASCE\)0733-9429\(1988\)114:7\(811\)](https://doi.org/10.1061/(ASCE)0733-9429(1988)114:7(811))
- Wahl, T. L., & Nikora, V. I. (2002). Discussion of “despiking acoustic Doppler velocimeter data” by Derek G. Goring and Vladimir I. Nikora. *Journal of Hydraulic Engineering*, 128(1), 117–126. [https://doi.org/10.1061/\(asce\)0733-9429\(2002\)128:1\(117\)](https://doi.org/10.1061/(asce)0733-9429(2002)128:1(117))
- Wallerstein, N., & Thorne, C. (2004). Influence of large woody debris on morphological evolution of incised, sand-bed channels. *Geomorphology*, 57(1–2), 53–73. [https://doi.org/10.1016/S0169-555X\(03\)00083-7](https://doi.org/10.1016/S0169-555X(03)00083-7)
- Wang, X. K., & Tan, S. K. (2007). Experimental investigation of the interaction between a plane wall jet and a parallel offset jet. *Experiments in Fluids*, 47(4), 551–562. <https://doi.org/10.1007/s00348-007-0263-9>
- Wang, X. K., & Tan, S. K. (2010). Environmental fluid dynamics – Jet flow. *Journal of Hydrodynamics*, 22(S1), 962–967. [https://doi.org/10.1016/S1001-6058\(10\)60067-4](https://doi.org/10.1016/S1001-6058(10)60067-4)
- Wang, X. K., & Tan, S. K. (2012). Flow around four circular cylinders in square configuration, 18th Australasian Fluid Mechanics Conference (pp. 3–7).
- Williamson, C. H. K. (1996). Vortex dynamics in the cylinder wake. *Annual Review of Fluid Mechanics*, 28(1), 477–539. <https://doi.org/10.1146/annurev.fl.28.010196.002401>
- Wohl, E. (2014). A legacy of absence: Wood removal in US rivers. *Progress in Physical Geography*, 38(5), 637–663. <https://doi.org/10.1177/0309133314548091>
- Wohl, E. (2017a). Bridging the gaps: An overview of wood across time and space in diverse rivers. *Geomorphology*, 279, 3–26. <https://doi.org/10.1016/j.geomorph.2016.04.014>
- Wohl, E. (2017b). Large wood in rivers, obo in environmental science. <https://doi.org/10.1093/OBO/9780199363445-0079>
- Wu, S., & Rajaratnam, N. (1995). Free jumps, submerged jumps, and wall jets. *Journal of Hydraulic Research*, 33(2), 197–212. <https://doi.org/10.1080/00221689509498670>
- Young, W. J. (1991). Flume study of the hydraulic effects of large woody debris in lowland rivers. *Regulated Rivers: Research & Management*, 6(3), 203–211. <https://doi.org/10.1002/rrr.3450060305>
- Zalewski, M., Magorzata, M., & Bayley, P. B. (2003). *Fish relationships with wood in large rivers*. In *The Ecology and Management of Wood in World Rivers* (Vol. 37). American Fisheries Society Symposium.
- Zhang, N., Rutherford, I. D., & Ghisalberti, M. (2020a). Effect of instream logs on bank erosion potential: A flume study with a single log. *Journal of Ecohydraulics*, 5(1), 43–56. <https://doi.org/10.1080/24705357.2019.1634499>
- Zhang, N., Rutherford, I. D., & Ghisalberti, M. (2020b). The effect of instream logs on bank erosion potential: A flume study with multiple logs. *Journal of Ecohydraulics*, 5(1), 57–70. <https://doi.org/10.1080/24705357.2019.1669495>
- Zong, L., & Nepf, H. (2011). Vortex development behind a finite porous obstruction in a channel. *Journal of Fluid Mechanics*, 691, 368–391. <https://doi.org/10.1017/jfm.2011.479>
- Zou, L., Lin, Y., & Lam, K. (2008). Large-eddy simulation of flow around cylinder arrays at a subcritical Reynolds number. *Journal of Hydrodynamics*, 20(4), 403–413. [https://doi.org/10.1016/S1001-6058\(08\)60074-8](https://doi.org/10.1016/S1001-6058(08)60074-8)
- Zou, L., Lin, Y., & Lu, H. (2011). Flow patterns and force characteristics of laminar flow past four cylinders in diamond arrangement. *Journal of Hydrodynamics*, 23(1), 55–64. [https://doi.org/10.1016/S1001-6058\(10\)60088-1](https://doi.org/10.1016/S1001-6058(10)60088-1)